Applied Physics A (2022) 128:622
https://doi.org/10.1007/s00339-022-05759-8

Applied Physics A
Materials Science & Processing

Structural analysis, dielectric relaxation, and AC electrical conductivity in $TlInSe_2$ thin films as a function of temperature and frequency

F. F. Al-Harbi[1] · A. A. A. Darwish[2,3,4] · Taymour A. Hamdalla[2,3,5] · K. F. Abd El-Rahman[6]

Received: 13 April 2022 / Accepted: 7 June 2022 / Published online: 29 June 2022

Abstract
Thallium indium di-selenium ($TlInSe_2$) is one of the most promising chalcogenide materials having a layered crystalline structure that has been nominated in different fields of industry. In our work, a film of $TlInSe_2$ has been fabricated using a coating unit. The morphology properties of $TlInSe_2$ have been investigated by atomic force microscopy (AFM). The Raman spectroscopy proved that there are identical spectra between the powder and the film, and they agreed with what was previously reported for the $TlInSe_2$ crystal. By AFM, it was found that the grain sizes and the roughness of $TlInSe_2$ film are 100 and 6.49 nm, respectively. The real (ε_1) and imaginary (ε_2) parts of complex dielectric permittivity and AC conductivity were measured in the frequency range of 42 Hz–5 MHz with a variation of temperature in the range from 303 to 443 K. The estimated values of ΔE_M and τ_o were found to be 0.321 eV and 2.28×10^{-10} s, respectively. The electrical conductivity of $TlInSe_2$ thin film increased by about 40% as the temperature increased from 303 to 443 K. On the contrary, the AC activation energy has decreased rapidly by about 54%.

Keywords Chalcogenide · Raman spectroscopy · AFM analysis · Dielectric relaxation · Electrical conductivity

1 Introduction

The chalcogenide materials are compounds that contain in their chemical structure at least one chalcogen ion, such as $TlGaTe_2$, $TlGaSe_2$, $TlInS_2$, $TlInTe_2$, and $TlInSe_2$ [1–3]. This group of compounds has special significant characteristics due to their high non-linear effects, high anisotropic properties, and high photo-conductivity properties [4]. Therefore, chalcogenide compounds are used in different fields of industry such as optoelectronics applications, semiconductor applications, etc. [5–7]. The performance of chalcogenide materials within optoelectronics applications is affected by the synthesis method, raw materials, and growth treatment. $TlInSe_2$ crystals consist of weak bonding between layers and separate layers with high ion–covalent bonding linking the atoms, while a weak van der Waals bonding linking the layers [8]. $TlInSe_2$ contains a high number of defects which will create a high density of localized states near the Fermi level [9]. Many recent scientific papers concerned with the optical, electrical, and photoelectrical properties of $TlGaSe_2$ have been published [10–12]. The XRD analysis of $TlInSe_2$ thin film has been previously investigated by Al-Ghamdi et al. [13]. The results showed that the prepared films are polycrystalline in the Tetragonal system. Also, they calculated the energy gap of $TlInSe_2$ and it is found that the direct energy gap (E_g^d), the indirect energy gap (E_g^{ind}), and the phonon energy (E_{ph}) are 1.89, 1.61, and 0.025 eV.

Many researchers studied the structure, electrical, and optical properties of $TlInSe_2$ single crystal [14, 15]. Qasrawi et al. [16] fabricated a high-performance p–n junction from $TlInSe_2$ at a low cost. The optical, electrical, and photoelectrical properties of $TlGaSe_2$ have been investigated by

✉ A. A. A. Darwish
aaadarwish@gmail.com

1 Department of Physics, College of Science, Princess Nourah bint Abdulrahman University, P.O. Box 84428, Riyadh 11671, Saudi Arabia

2 Department of Physics, Faculty of Science, University of Tabuk, Tabuk 71491, Saudi Arabia

3 Nanotechnology Research Unit, Faculty of Science, University of Tabuk, Tabuk 71491, Saudi Arabia

4 Department of Physics, Faculty of Education at Al-Mahweet, Sana'a University, Al-Mahweet, Yemen

5 Department of Physics, Faculty of Science, Alexandria University, Alexandria, Egypt

6 Department of Physics, Faculty of Education, Ain Shams University, Roxy, Cairo 11757, Egypt

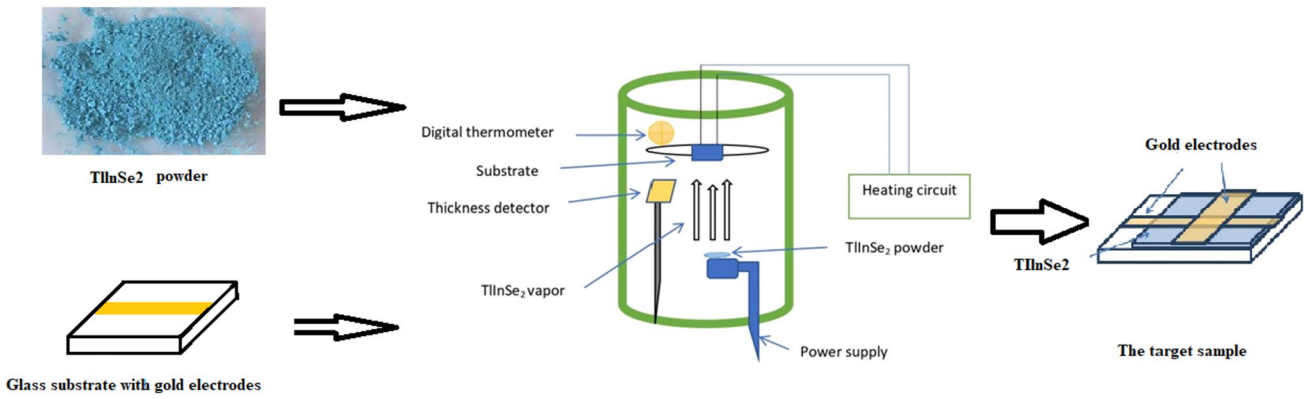

Scheme 1 Experimental design for $TlInSe_2$ thin films with gold electrodes for electrical measurements

Kalomiros et al. [17]. Ashraf et al. [18] used $TlGaSe_2$ thin film-based photo-detector as visible-light photo-detector. $TlGaSe_2$ as a wide broad-spectral response phototransistor has been investigated by Yang et al. [19]. The conduction mechanism and the electric properties of $TlInS_2$:Cu crystals have been measured by El-Nahass et al. [20]; they found that the ac conductivity increased linearly with temperature while ac activation energy decreased with increasing frequency. The dielectric constants and AC electrical of $TlInS_2$ films are measured at temperatures ranging from 373 to 473 K and frequencies ranging from 0.5 to 200 kHz [21]. The AC conductivity rises as the temperature rises and follows the universal power. Furthermore, at high temperatures, the dielectric constants exhibit high values because of the presence of interface charges formed at the interfacial surface.

As a result of our previous introduction, all the researchers studied the $TlInSe_2$ as a single crystal material. Here in our work, we fabricated a $TlInSe_2$ as a thin film using a temperature substrate and will study in detail its morphology. Then, we will investigate dielectric constants, and AC conductivity of $TlInSe_2$ films as a function of temperature and frequency. We hope the results of the present paper would remarkably provide valuable information for optoelectronic applications of $TlInSe_2$ films.

2 Experimental details

Sigma Aldrich supplied all chemicals (Tl, In, and Se with 99.999% pure elements). $TlInSe_2$ materials were created by combining stoichiometric components in silica vacuum ampoules with a lower tip. To prevent the ampoule from exploding, it was heated in a gradient temperature oven, where Selenide condenses in the cold end and reacts slowly with hot elements in the hot end. The ampoule was kept at 1173 K for 10 h after the reaction was completed to ensure homogeneity. The materials slowly cooled down in the cold zone over a couple of days.

The thermal evaporation method was used to create $TlInSe_2$ films under a vacuum of 1.34×10^{-6} mbar utilizing an HHV Auto 306 coating unit. Scheme 1 shows the preparation technique of $TlInSe_2$ films on a heated substrate. The films were grown on glass substrates that had been optically and ultrasonically cleaned. To achieve homogeneous prepared films at a separation of 25 cm above the evaporator, the glass substrate was settled onto a rotatable holder. The substrates were kept at 573 K. The temperature of the substrate has a significant impact on the crystal size and morphology of the films. The quartz crystal monitor was used to control the deposition rate at 10 Å/s as well as the film thickness. The film thickness was then measured using the interferometric method and found to be 300 nm. A sandwich formation was accomplished from a $TlInSe_2$ film fused between two gold electrodes.

Raman spectroscopy (CCD-chip, DPSS-Laser with 532 nm, and spectral resolution 2.3 cm^{-1}) was used to investigate the vibrational properties of these films. Atomic force microscopy (AFM) model NT-MDT was used to investigate surface topography, grain size, and surface roughness. The AC conductivity, as well as dielectric measurements of $TlInS_2$ film, were measured by the Hioki RLC meter (model 3532 Hitester). The capacitance (C), impedance (Z), and the phase angle (φ) were estimated in a frequency range of 42 Hz–5 MHz. A Type K thermocouple (Chromel/Alumel) was used to measure the sample temperatures (290–373 K).

3 Results and discussion

3.1 Raman shift analysis

The spectroscopy of Raman shift is an advanced technique used to diagnose the rotational, vibrational, and other states

in a molecular system, and also it can provide essential information on the chemical composition of materials. Raman spectrometry data is shown in Fig. 1 for $TlInSe_2$ powder and film. It is clear from Fig. 1 that the Raman spectra of the $TlInSe_2$ contain five peaks at (27, 56, 91, 156, and 179 cm^{-1}) for powder, while (27, 56, 94, 169, 181 cm^{-1}) for films. Matching in the Raman spectra of the powder and film confirms the effectiveness of preparing these films by thermal evaporation on substrates heated at 573 K. The observed frequencies are consistent with the previously reported Raman results for $TlInSe_2$ crystal [22, 23]. The comparison of $TlInSe_2$ vibrational frequencies is given in Table 1.

3.2 AFM analysis

For the surface scanning that has sub-nanometer-scale resolution, AFM has been utilized to investigate the $TlInSe_2$ film. AFM image of the surface of our investigated film has been introduced in Fig. 2a. The AFM pictures showed different peaks and valleys and they are spreading consistently within the checking region. Figure 2b illustrates the diameter distribution diagram of $TlInSe_2$ film. The grain sizes and the roughness of $TlInS_2$ thin film are 100 and 6.49 nm, respectively. The values of $TlInSe_2$ grain size and roughness are in correspondence with that obtained in [24, 25]

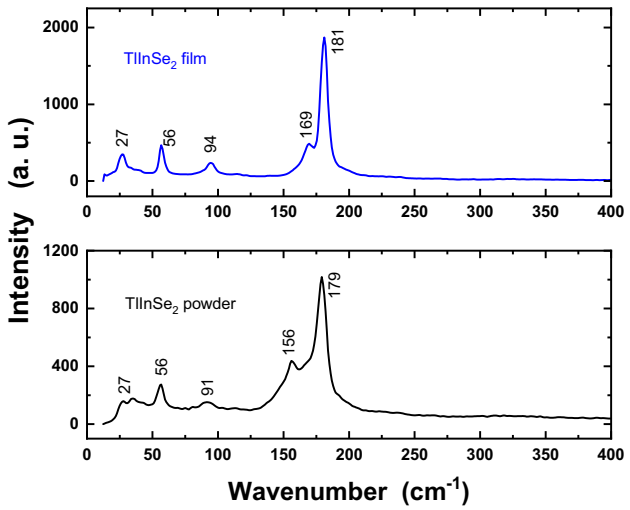

Fig. 1 Raman scattering spectra of $TlInSe_2$ powder and film

3.3 Dielectric relaxation

Dielectric spectroscopy is an important parameter that the dielectric properties of a medium as a function of frequency [26]. This spectroscopy depends on the interaction of an external field with the electric dipole moment of the sample. It is worth mentioning that the dielectric mechanisms can be divided into relaxation and resonance processes. The electric modulus can be used as a power examination tool for specific investigation of the dielectric properties of the material. Such studies were conducted at different frequencies and temperatures, to distinguish between long-range charge transport and local dielectric relaxation. Hence, applying the electric modulus can eliminate the relaxation contribution of impurity conduction effects, space charge injection phenomenon, and electrode effect, enabling the main source of electrical polarization in the material to be determined [27]. To understand the origin and nature of the dielectric properties of the materials, dielectric relaxation must be studied in detail. The function of the complex dielectric could be calculated using [21]:

$$\varepsilon^* = \varepsilon_1 + i\varepsilon_2, \tag{1}$$

$$\varepsilon_1 = C\frac{d}{\varepsilon_o A}, \quad \varepsilon_2 = \varepsilon_2 \tan(\delta), \tag{2}$$

where ε_o is the free space permittivity, ε_1 is the dielectric constant and ε_2 is the dielectric loss. d is the film thickness, A is the cross-section area, and $\delta = 90 - \varphi$.

Figure 3a, b depicts the change of ε_1 and ε_2 with ln ω under the effect of temperature variation between 303 and 443 K, respectively. As seen in Fig. 3a, b, ε_1 and ε_2 decrease with increasing frequency. The change in ε_1 and ε_2 has been previously recorded for similar compounds such as $TlInS_2$ and $TlInS_2$:Cu [28, 29]. This behavior may be related to the dielectric constant concept that is associated with the material polarization under the AC field effect [30]. At the low frequencies range. The ionic, electronic, dipolar, or orientation and space charge polarizations are highly active. Ionic polarization occurs as a result of the displacement of positive and negative ions relative to one another. Dipole polarization is caused by the presence of molecules with permanent electric dipole moments that can change direction

Table 1 The vibrational frequencies of $TlInSe_2$ powder and films were compared to those found in the literature

No.	$TlInSe_2$ powder	$TlInSe_2$ film	$TlInSe_2$ crystal [16]	$TlInSe_2$ crystal [17]
1	27	27	28 (A_{2u})	30 (E_g)
2	56	56	54 (E_u)	48 (E_u)
3	91	94	98 (E_u)	98 (E_u)
4	156	169	–	–
5	179	181	179 (A_{2u})	184 (A_{1g})

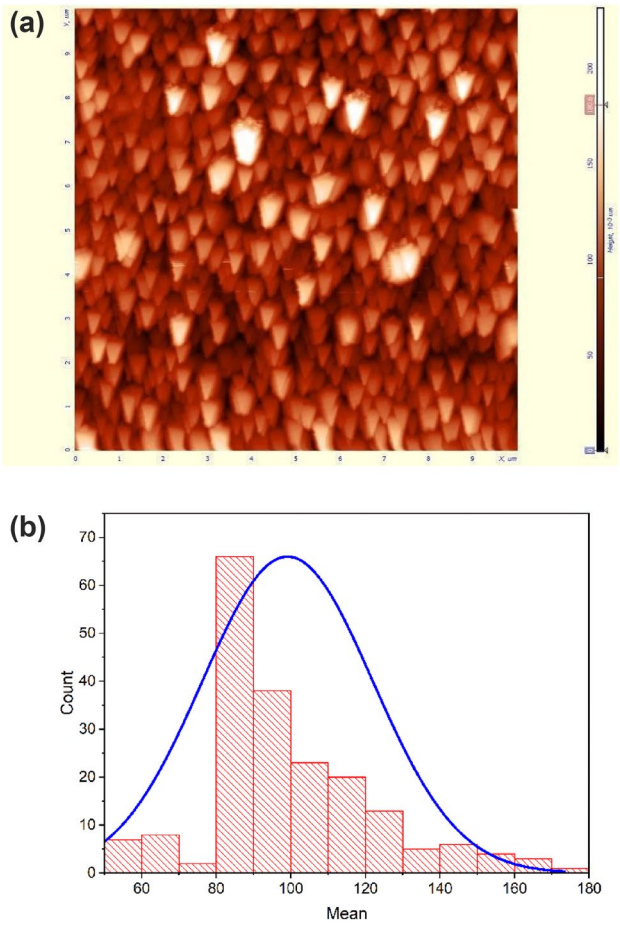

Fig. 2 **a** AFM image and **b** diameter distribution diagram for $TlInSe_2$ film

in the direction of the applied electric field. The resistance of charge carriers traveling through interfaces causes polarization of space charge. The sum of these polarizations is the total polarization of insulating material. As frequency increases, orientation polarization takes longer than other types of polarization, and dipoles cannot rotate fast enough to keep up with the oscillations of the field, so their oscillations lag behind the field. With increasing frequency, the dipole will not be able to follow the field and the directional polarization will stop, so ε decreases and approaches a constant value at high frequencies because of the polarization of the space charge. Also, as the temperature increases the values of ε increase, which can be attributed to the thermal electron motion that acts to increase the electrons' orientation and polarization [31].

We use electrophoresis as a tool to further explore the dielectric relaxation of the materials. Such studies, performed under different temperatures and frequencies, enable us to distinguish between local dielectric relaxation and long-range charge transport. As a result, by using electrical units, we get rid of the relaxation contribution of space charge injection phenomena, impurity conduction effects, and the nature of the electrode, and thus the main source of electric polarization in this material can be estimated. In the way for studying the relaxation process of the $TlInS_2$ thin film, we have to study the electric complex modulus, M, using the following equation [32]:

$$M = M_1 + jM_2, \tag{3}$$

$$M_1 = \varepsilon_1 \times \left[(\varepsilon_1)^2 + (\varepsilon_2)^2\right]^{-1}, \quad M_2 = \varepsilon_2 \times \left[(\varepsilon_1)^2 + (\varepsilon_2)^2\right]^{-1}, \tag{4}$$

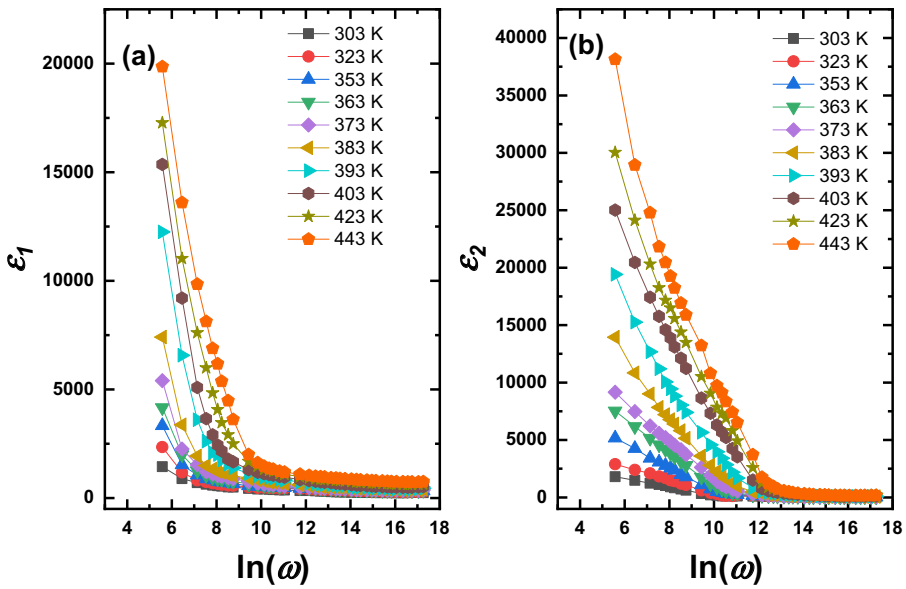

Fig. 3 The frequency and temperature dependence of ε_1 and ε_2 for $TlInSe_2$ film

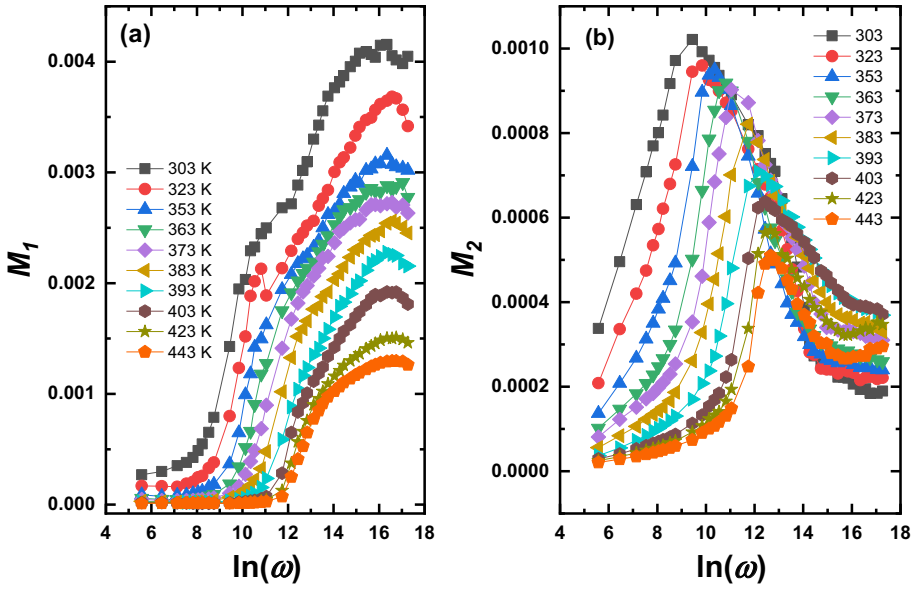

Fig. 4 The frequency and temperature dependence of M_1 and M_2 for $TlInSe_2$ film

where M_1 is the real part, while M_2 is the imaginary part of the dielectric modulus. Figure 4 displays the frequency dependence of M_1 and M_2 at different temperatures for $TlInSe_2$ film.

It is clear from Fig. 4a that, for all the estimated temperatures, M_1 increases as ln ω increases and approaches zero at low frequencies. In the temperature ranges studied, such behavior confirmed the presence of an appreciable electrode and/or ionic polarization [33]. As we can notify from Fig. 4b, the values of M_2 increase as ln ω increases till reaching an inverted point (ω_{max}). The region of frequency less than the ω_{max} value defines the range over which charge carriers can travel over long distances. For frequencies greater than the ω_{max} value, the carriers appear to be confined to the potential well, but they become mobile after a short distance [34]. Additionally, the position of ω_{max} increases with increasing temperature. This finding demonstrates that the thermal activation process has a major impact on the relaxing mechanism. Also, when the temperature is increased, the orientation of the electron is changed and this leads to increases in the polarization. The relaxation time, τ_{max}, ($\tau_m = \omega_{max}{}^{-1}$) is given by the Arrhenius equation [35]:

$$\tau_{max} = \tau_0 \exp\left(\frac{\Delta E_M}{k_B T}\right), \tag{5}$$

where k_B is the Boltzmann constant, τ_o is the pre-exponent factor, and ΔE_M is the activation energy of relaxation time. Figure 5 shows the variation of ln τ_{max} with 1000/T for $TlInSe_2$ films. The estimated values of ΔE_M and τ_o were found to be 0.321 eV and 2.28×10^{-10} s, respectively.

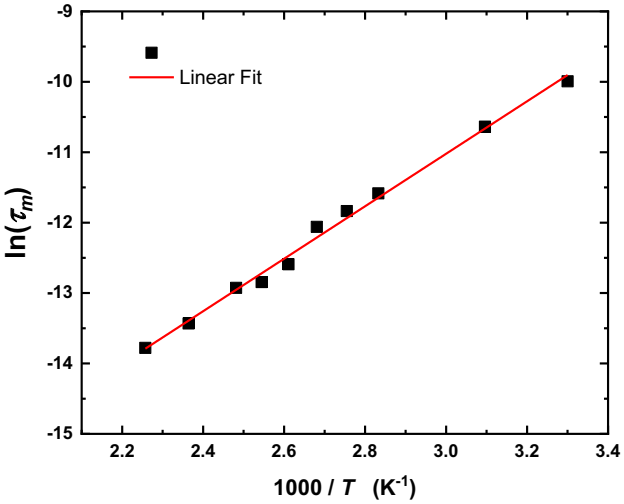

Fig. 5 The variation of ln(τ_m) with 1000/T for $TlInSe_2$ films

3.4 The electrical conductivity analysis

It is well known that electrical conductivity is completely related to the internal structure of the conductive materials. To obtain the values of total conductivity (σ_t), the following equations were utilized:

$$\sigma_t = \frac{d}{ZA}, \tag{6}$$

where Z is the material impedance. Figure 6 shows the frequency and temperature dependence of σ_t for $TlInSe_2$ film. It is worth mentioning that the total conductivity of $TlInS_2$ film increases with increasing frequency and temperature.

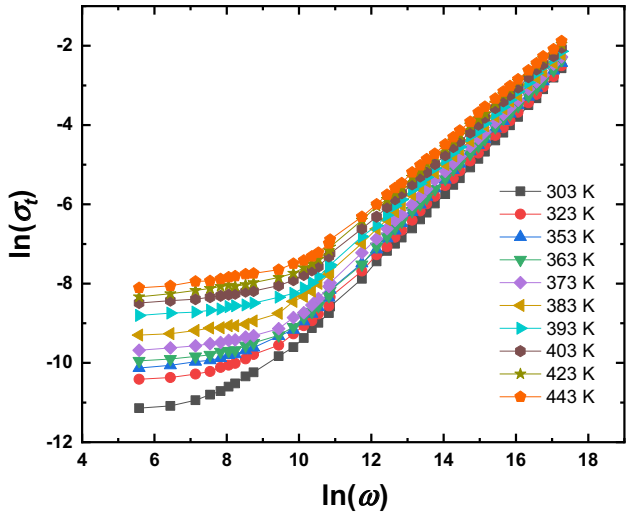

Fig. 6 The frequency and temperature dependence of σ_t for $TlInSe_2$ film

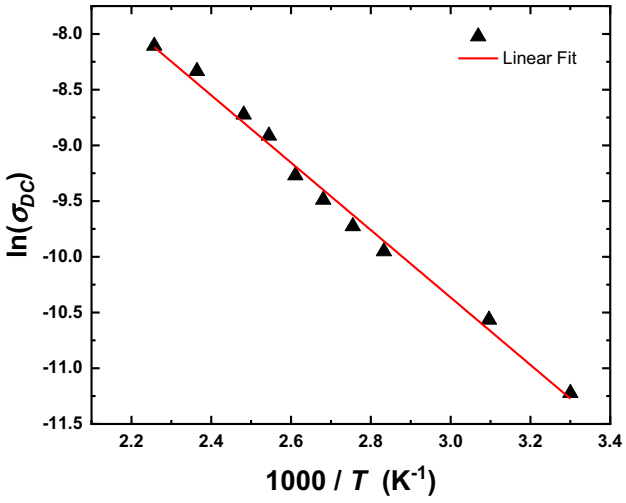

Fig. 7 The relation between $\ln(\sigma_{DC})$ and $1000/T$ for $TlInSe_2$ film

This figure also indicates that at low frequencies, σ_t is practically constant. On the other hand, the overall conductivity increases as a function of the frequency's power law over a given range of frequencies. For this case, Jonscher's universal dynamic response (UDR) is widely used to describe the total electrical conductivity, σ_t, as follows [36]:

$$\sigma_t = \sigma_{DC} + \sigma_{AC}, \tag{7}$$

where σ_{DC} and σ_{AC} are the DC conductivity and AC conductivity, respectively. As a result, σ_{DC} is the predominant component in the low-frequency regime. This allows us to explore the influence of temperature on σ_{DC}, that cloud be calculated by extrapolating σ_t data to zero frequency.

According to Arrhenius's relation, the DC conductivity of $TlInSe_2$ film is defined by [24]:

$$\sigma_{DC} = \sigma_{o1} \exp\left(\frac{-\Delta E}{k_B T}\right), \tag{8}$$

where σ_{o1} is a constant and ΔE is the activation energy. Figure 7 shows the relation between ln σ_{DC} and $1000/T$ for $TlInSe_2$ film. Hence, the ΔE value is estimated to be 0.261 ± 0.25 eV.

The conductivity of alternating current, which is made up of total conductivity, is dominant in high-frequency systems. The relation of the conductivity of the material could be calculated by Jonscher's power equation [37]:

$$\ln(\sigma_{AC}) = \ln \ln (B) + s \ln (\omega), \tag{9}$$

where B is constant and s is the frequency component. Figure 8 depicts the relation between $\ln(\sigma_{AC})$ and $\ln(\omega)$ for $TlInSe_2$ film at some constant temperatures.

To comprehend the $TiInSe_2$ film's AC conduction mechanism, the parameter s presenting information about the AC conduction mechanism of the $TlInSe_2$ thin film may be obtained from the slope of the $\ln(\sigma_{AC})$ vs. $\ln(\omega)$ plot. The values of the frequency exponent are shown in Fig. 9a as a function of temperature. Note that the value of s decreases with increasing temperature and approaches 0.86 at 443 K as the correlated barrier hopping (CBH) model [27] is the most appropriate mechanism to characterize the AC conductivity of $TlInSe_2$ in the scope of the temperature study. In the CBH model, charge carriers are supposed to jump over the potential barrier separating neighboring local sites. The frequency exponent s for the hopping model is given by [38, 39]:

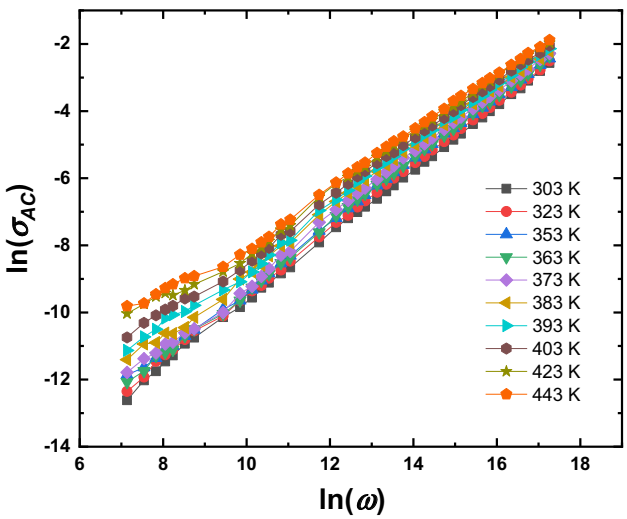

Fig. 8 The frequency and temperature dependence of σ_{AC} for $TlInSe_2$ film

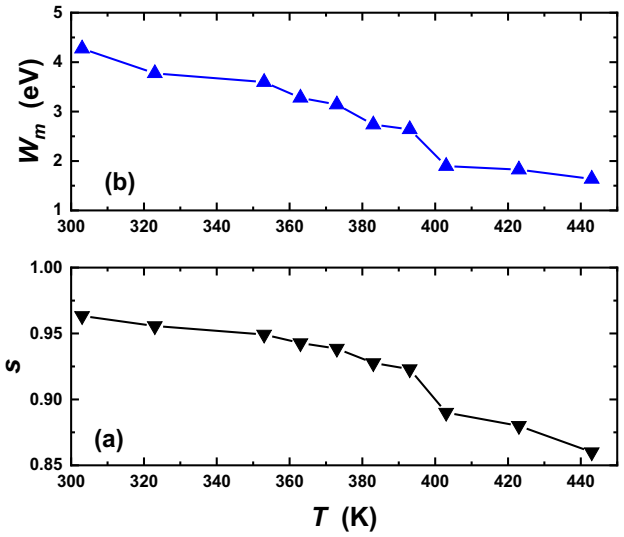

Fig. 9 Temperature dependence of the frequency exponent, *s*, and the maximum barrier height for $TlInSe_2$ film

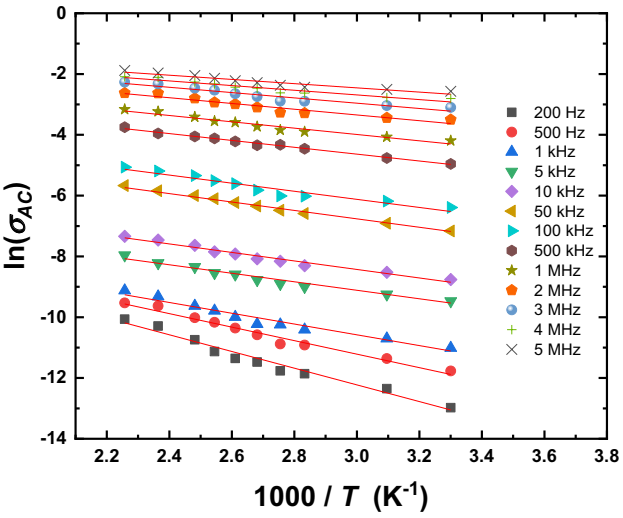

Fig. 10 The relation between ln(σ_{AC}) and 1000/*T* for $TlInSe_2$ film at different frequencies

$$s = 1 - \frac{6k_B T}{W_m}, \tag{10}$$

where W_m is the maximum barrier height which can be defined as the amount of energy required to transfer an electron from its local to its indeterminate level. Figure 9b shows the W_m values as a function of temperature. It has been observed that W_m decreases as temperature rises. As a result, the exponent decreases as the temperature rises because increasing the temperature will act to increase the energy between localized and delocalized states.

In addition, the AC conductivity is temperature dependent and, thus, has a thermal activating effect and the Arrhenius relation could be utilized to calculate the activation energy, ΔE_{AC}, according to the following relation [35]:

$$\sigma_{AC} = \sigma_o \exp\left(\frac{-\Delta E_{ac}}{k_B T}\right), \tag{11}$$

where σ_o is the pre-exponential factor. Figure 10 depicts the relation between ln σ_{AC} and 1000/*T* for $TlInSe_2$ film at different frequencies. ln(σ_{AC}) has large values at higher temperatures, which could be related to the greater quantity of charges, which leads to increased hopping. According to the hopping conduction process, the increase in conductivity with rising temperature is attributed to an increase in the drift velocity of thermally activated electrons for charge carriers. The activation energy for the $TlInSe_2$ film is calculated from the linear fit slopes of the straight lines in Fig. 10 and shown in Fig. 11. The values of ΔE_{AC} decreased with increasing frequency. This behavior is related due to an increase in the frequency that boosts the electronic jumps between local states, and thus the activation energy decreases with increasing frequency [28].

4 Conclusions

Chalcogenide materials based on selenium are very applicable materials that have been used in different fields of industry such as fuel cell, battery, photovoltaic, etc. In our work, $TlInSe_2$ films are deposited on substrate temperature using a coating unit. Raman spectra of $TlInSe_2$ powder and film confirm the effectiveness of preparing these films by thermal evaporation on substrates heated at 573 K. Atomic force microscopy image confirms that the $TlInSe_2$ film has grain

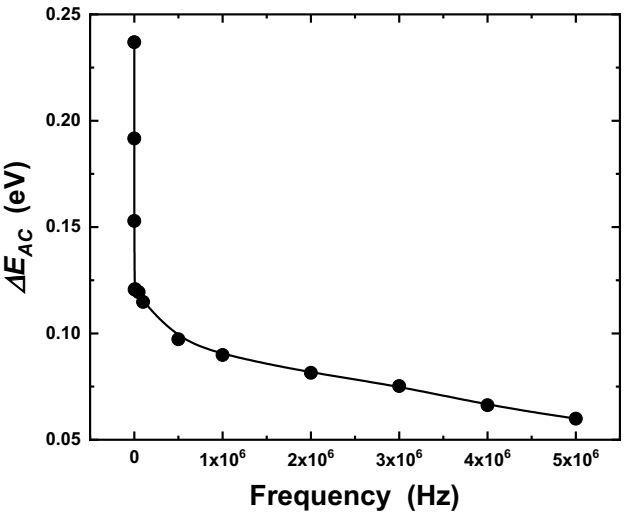

Fig. 11 Frequency dependence of ΔE_{ac} of $TlInSe_2$ film

sizes and the roughness of 100 nm and 6.49 nm, respectively. The dielectric properties show that at low frequencies, there is a large dispersion of permittivity constants, which can be attributed to distinct polarizations, and at high frequencies, the dielectric constant approaches a constant value due to space charge polarization. The real part of the electrical modulus rises with frequency and falls to zero at low frequencies. For some temperatures, the patterns of the imaginary part of the electrical modulus showed peaks. The relaxation processes' activation energy was determined to be 0.321 eV. The AC and DC electrical conductivity is conducted in the temperature range of 303–443 K and found that they have a thermal activating effect. Also, the correlated barrier hopping model is the most appropriate mechanism to characterize the AC conductivity of $TlInSe_2$ film in the scope of the temperature study.

Acknowledgements The authors express their gratitude to Princess Nourah bint Abdulrahman University Researchers Supporting Project (Grant no. PNURSP2022R55), Princess Nourah bint Abdulrahman University, Riyadh, Saudi Arabia.

Author contributions All authors contributed equally throughout the whole manuscript.

Funding The authors had listed the support of relevant funds in the acknowledgment section.

Data availability statement The authors confirm that the datasets generated during and analyzed during the current study are available from the corresponding author on reasonable request.

Declarations

Conflict of interest The authors declare that there is no conflict of interest in the manuscript.

References

1. A. Aydinli, N.M. Gasanly, I. Yilmaz, A. Serpengüzel, Radiative donor-acceptor pair recombination in TlInS2 single crystals. Semicond. Sci. Technol. **14**, 599 (1999)
2. M. Isik, M. Terlemezoglu, N.M. Gasanly, R.F. Babayeva, Vibrational modes in $(TlGaS_2)_x$–$(TlGaSe_2)_{1-x}$ mixed crystals by Raman measurements: compositional dependence of the mode frequencies and line-shapes. J. Mater. Sci. Mater. Electron. **31**, 14330–14335 (2020)
3. SKh. Umarov, I. Nuritdinov, Zh. Ashurov, F.K. Khallokov, Resistivity and tensoresistive characteristics of $TlInSe_2$–$CuInSe_2$ solid solutions. Tech. Phys. **64**, 183–186 (2019)
4. M. Shpotyuk, A. Kovalskiy, R. Golovchak, O. Shpotyuk, Phenomenology of γ-irradiation-induced changes in optical properties of chalcogenide semiconductor glasses: a case study of binary arsenic sulfides. J. NonCryst. Solids **498**, 315–322 (2018)
5. A. Rahmana, M.M. Khan, Chalcogenides as photocatalysts. New J. Chem. **45**, 19622–19635 (2021)
6. A.A.A. Darwish, T.A. Hamdalla, E.F.M. El-Zaidia, T.A. Hanafy, S.A.M. Issa, I.S. Yahia, Thin films of nanostructured gallium (III) chloride phthalocyanine deposited on FTO: Structural characterization, optical properties, and laser optical limiting. Phys. B Condens. Matter **593**, 412321 (2020)
7. P. Koštál, J. Shánělová, J. Málek, Viscosity of chalcogenide glass-formers. Int. Mater. Rev. **65**, 63–101 (2020)
8. M. Çaydaşı, M.F. Mintaş, Y.M. Chumakov, S. Volz, A. Cengiz, M.H.Y. Seyidov, A study of thermoelectric performance of TlGaSe2 layered dichalcogenides from first-principles calculations: vacancy defects modeling and engineering. Phys. Status Solidi B **259**, 2100409 (2022)
9. R.M. Sardarli, F.T. Salmanov, N.A. Alieva, R.M. Abbasli, Impedance spectroscopy of $(TlGaSe_2)_{1-x}(TlInSe_2)_x$ solid solutions in radio frequency range. Mod. Phys. Lett. B **34**, 2050113 (2020)
10. R.S. Madatov, Sh.G. Gasimov, S.S. Babayev, A.S. Alekperov, I.M. Movsumova, S.H. Jabarov, Features of the electrical-conductivity mechanism in γ-irradiated TlInSe2 single crystals under hydrostatic pressure. Semiconductors **54**(10), 1180–1184 (2020)
11. M. Isik, S. Delice, N.M. Gasanly, Optical properties of $TlGa_xIn_{1-x}Se_2$-layered mixed crystals ($0.5 \leq x \leq 1$) by spectroscopic ellipsometry, transmission, and reflection measurements. Philos. Mag. **94**, 2623–2632 (2014)
12. M. Isik, A. Karatay, N.M. Gasanly, Structural and optical characteristics of thermally evaporated TlGaSe2 thin films. Opt. Mater. **124**, 112018 (2022)
13. S.A. Al-Ghamdi, A.A.A. Darwish, T.A. Hamdalla, A.O.M. Alzahrani, S. Khasim, S.I. Qashou, K.F. Abd El-Rahm, Preparation of TlInSe2 thin films using substrate temperature: characterization, optical and electrical properties. Opt. Mater. **129**, 112514 (2022)
14. A.A. Attia, M.A.M. Seyam, S.S. Nemr, AC conductivity and dielectric relaxation properties of bulk TlInSe2 prepared from single crystal. J. Mater. Sci. Mater. Electron. **29**, 7325–7332 (2018)
15. M. Isik, N.M. Gasanly, Effect of thallium (Tl) substitution for indium (In) on ellipsometric characteristics of TlInSe2 single crystals. Mater. Sci. Semicond. Process. **134**, 106005 (2021)
16. A.F. Qasrawi, F.G. Aljammal, N.M. Taleb, N.M. Gasanly, Design and characterization of TlInSe2 varactor devices. Phys. B Condens. Matter **406**, 2740–2744 (2011)
17. J.A. Kalomiros, N. Kalkan, M. Hanias, A.N. Anagnostopoulos, K. Kambas, Optical and photoelectric properties of TlGaSe2 layered crystals. Solid State Commun. **96**, 601–607 (1995)
18. I.M. Ashraf, M. Shkir, S. AlFaify, F. Abdel-Wahab, A.M. Ali, M.A. Sebak, M.S. Awad Al-Juman, M.F. Sanaa, Development and characterization of TlGaSe2 thin film-based photodetector for visible-light photodetector applications. Opt. Mater. **103**, 109834 (2020)
19. S. Yang, M. Wu, H. Wang, H. Cai, L. Huang, C. Jiang, S. Tongay, Ultrathin ternary semiconductor TlGaSe2 phototransistors with broad-spectral response. 2D Mater. **4**, 035021 (2017)
20. M.M. El-Nahass, M.M. Sallam, S.A. Rahman, E.M. Ibrahim, Solid State Sci. **8**, 488–499 (2006)
21. A. El-Ghandour, N.A. El-Ghamaz, M.M. El-Nahass, H.M. Zeyada, Temperature and frequency dependence outline of DC electrical conductivity, dielectric constants, and AC electrical conductivity in nanostructured TlInS2 thin films. Physica E **105**, 13–18 (2019)
22. N.M. Gasanly, A.F. Goncharov, B.M. Dzhavadov, N.N. Melnik, V.I. Tagirov, E.A. Vinogradov, Vibrational spectra of TlGaTe2, TlInTe2, and TlInSe2 layer single crystals. Phys. Status Solidi B **97**, 367 (1980)
23. O. Madelung, U. Rossler, M. Schulz (ed.), Non-tetrahedrally bonded elements and binary compounds, vol. 41 (Springer, Berlin, 1998), p. p1
24. I. Guler, N. Gasanly, Structural and optical properties of thermally annealed thallium indium disulfide thin films. Thin Solid Films **704**, 137985 (2020)

25. S.A. Mahmoud, A. Shereen, A.T. Mou'ad, Structural and optical dispersion characterization of sprayed nickel oxide thin films. J. Mod. Phys. **2011** (2011) 1178–1186
26. S.O. Nelson, Dielectric properties measurement techniques and applications. Trans. ASAE **42**(2), 523 (1999)
27. A.A.A. Darwish, S.R. Alharbi, M.M. Hawamdeh, A.M. Alsharari, S.I. Qashou, Dielectric properties and AC conductivity of organic films of Copper(II) 2,9,16,23-Tetra-tert-butyl-29H,31Hphthalocyanine. J. Electron. Mater. **49**, 1787–1793 (2020)
28. M.M. El-Nahass, S.B. Youssef, H.A.M. Ali, A. Hassan, Electrical conductivity and dielectric properties of TlInS2 single crystals. Eur. Phys. J. Appl. Phys. **55**, 10101 (2011)
29. M.M. El-Nahass, H.A.M. Ali, E.F.M. El-Zaidia, Characteristics of dielectric properties and conduction mechanism of TlInS2: Cu single crystals. Physica B **431**, 54–57 (2013)
30. B. Angadi, P. Victor, V.M. Jali, M.T. Lagare, R. Kumar, S.B. Krupanidhi, Ac conductivity studies on the Li irradiated PZT and SBT ferroelectric thin films. Mater. Sci. Eng. B **100**, 93–101 (2003)
31. A.F. Qasrawi, N.M. Gasanly, Optical properties of TlInS2 layered single crystals near the absorption edge. J. Mater. Sci. **41**, 3569–3572 (2006)
32. A.S. Alaeddin, P. Poopalan, AC conductivity and dielectric relaxation behavior of sol-gel $BaxSr_{1-x}TiO_3$ thin films. J. Mater. Sci. Technol. **27**, 802–808 (2011)
33. M.P. Dasari, K.S. Rao, P.M. Krishna, G.G. Krishna, Barium strontium bismuth niobate layered perovskites: dielectric, impedance, and electrical modulus characteristics. Acta Phys. Pol. A **119**, 387 (2011)
34. A. Moguš-Milanković, A. Šantić, V. Liĉina, D.E. Day, Dielectric behavior and impedance spectroscopy of bismuth iron phosphate glasses. J. NonCryst. Solids **351**, 3235 (2005)
35. S.I. Qashou, A.A.A. Darwish, M. Rashad, Z. Khattari, AC electrical conductivity and dielectric relaxation studies on n-type organic thin films of N,N′-Dimethyl-3,4,9,10-perylenedicarboximide (DMPDC). Physica B **525**, 159–163 (2017)
36. A.A.A. Darwish, A.M. Hassanien, T.A. Hanafy, M.M. El-Nahass, On the nature of bulk electrical relaxation in 4-tricyanovinyl-N,N-diethylaniline (TCVA). Synth. Met. **199**, 339–344 (2015)
37. A.K. Jonscher, Dielectric relaxation in solids. J. Phys. D Appl. Phys. **32**, R57 (1999)
38. S.R. Elliott, A.c. conduction in amorphous chalcogenide and pnictide semiconductors. Adv. Phys. **36**, 135–217 (1987)
39. G.E. Pike, ac Conductivity of scandium oxide and a new hopping model for conductivity. Phys. Rev. B **6**, 1572 (1972)